HOW DO VISION TRANSFORMERS WORK?

Anonymous authors
Paper under double-blind review

ABSTRACT

The success of multi-head self-attentions (MSAs) for computer vision is now indisputable. However, little is known about how MSAs work. We present various explanations to help better understand the nature of MSAs. In particular, we demonstrate the following properties of MSAs and Vision Transformers (ViTs): ❶ MSAs improve not only accuracy but also generalization by flattening the loss landscapes. Such improvement is primarily attributable to their data specificity, not long-range dependency. On the other hand, ViTs suffers from the non-convex losses. Large datasets and loss landscape smoothing methods alleviate this problem. ❷ MSAs and Convs exhibit opposite behaviors. For example, MSAs are low-pass filters, but Convs are high-pass filters. Therefore, MSAs and Convs are complementary. ❸ Multi-stage neural networks behave like a series connection of small independent models. In addition, MSAs at the end of a stage play a key role in prediction. Based on these insights, we propose AlterNet, a model in which Conv blocks at the end of a stage are replaced with MSA blocks. AlterNet outperforms CNNs not only in large data regime but also in small data regime.

1 INTRODUCTION

There is limited understanding of multi-head self-attentions (MSAs), although they are now ubiquitous in computer vision. The most widely accepted explanation for the success of MSAs is their weak inductive bias and capture of long-range dependencies (See, e.g., (Dosovitskiy et al., 2020; Naseer et al., 2021; Tuli et al., 2021; Yu et al., 2021; Mao et al., 2021; Chu et al., 2021)). Yet because of their over-flexibility, Vision Transformers (ViTs)—neural networks (NNs) consisting of MSAs—have been known to have a tendency to overfit training datasets, consequently leading to poor predictive performance in small data regimes, e.g., image classification on CIFAR (Krizhevsky et al., 2009). However, we show that the explanation is poorly supported.

1.1 RELATED WORK

Self-attentions (Vaswani et al., 2017; Dosovitskiy et al., 2020) aggregate (spatial) tokens with normalized importances:

$$\boldsymbol{z}_j = \sum_i \texttt{Softmax}\left(\frac{\boldsymbol{Q}\boldsymbol{K}}{\sqrt{d}}\right)_i \boldsymbol{V}_{i,j} \tag{1}$$

where $\boldsymbol{Q}$, $\boldsymbol{K}$, and $\boldsymbol{V}$ are query, key, and value, respectively. d is the dimension of query and key, and $\boldsymbol{z}_j$ is the j-th output token. From the perspective of convolutional neural networks (CNNs), MSAs are a transformation of all feature map points with large-sized data-specific kernels. Therefore, MSAs are at least as expressive as convolutional layers (Convs) (Cordonnier et al., 2019), although this does not guarantee that MSAs will behave like Convs.

Is the weak inductive bias of MSA, such as modeling long-range dependencies, beneficial for the predictive performance? To the contrary, appropriate constraints may actually help a model learn strong representations. For example, local MSAs (Yang et al., 2019; Liu et al., 2021; Chu et al., 2021), which calculate self-attention only within small windows, achieve better performance than global MSAs not only on small datasets but also on large datasets, such as ImageNet-21K (Russakovsky et al., 2015).

In addition, prior works observed that MSAs have the following intriguing properties: (1) MSAs improve the predictive performance of CNNs (Dai et al., 2021; Guo et al., 2021; Srinivas et al., 2021),

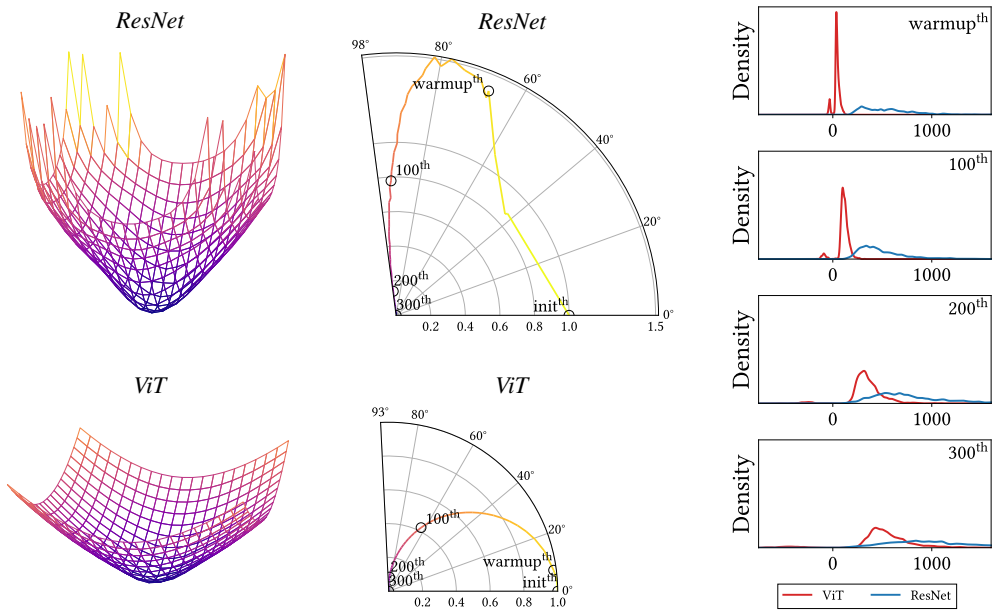

(a) Loss landscape visualizations (b) Trajectories in polar coordinate (c) Hessian max eigenvalue spectra

Figure 1: **Three different aspects consistently show that MSAs flatten loss landscape**. *Left*: Loss landscape visualizations show that ViT has a flatter loss (NLL $+ \ell_2$ regularization) than ResNet. *Middle*: ViT converges to the optimum along a smooth trajectory. In the polar coordinate, $r_t = \frac{||\Delta \boldsymbol{w}_t||}{||\Delta \boldsymbol{w}_{\text{init}}||}$ and $\theta_t = \cos^{-1}\left(\frac{\Delta \boldsymbol{w}_t \cdot \Delta \boldsymbol{w}_{\text{init}}}{||\Delta \boldsymbol{w}_t|| \, ||\Delta \boldsymbol{w}_{\text{init}}||}\right)$ where $\Delta \boldsymbol{w}_t = \boldsymbol{w}_t - \boldsymbol{w}_{\text{optim}}$ and $\boldsymbol{w}_t$ is NN weight at t^{th} epoch. $\boldsymbol{w}_{\text{init}}$ and $\boldsymbol{w}_{\text{optim}}$ are the weights at initialization and optimum. *Right*: The magnitude of the Hessian eigenvalues of ViT is smaller than that of ResNet. See Fig. 4 for a more detailed analysis.

and ViTs predict well-calibrated uncertainty (Minderer et al., 2021). (2) ViTs are robust against data corruptions, image occlusions (Naseer et al., 2021), and adversarial attacks (Shao et al., 2021; Bhojanapalli et al., 2021; Paul & Chen, 2021; Mao et al., 2021), and particularly robust against high-frequency noise (Shao et al., 2021). (3) MSAs closer to the last layer significantly improve predictive performance (Graham et al., 2021; Dai et al., 2021; Xiao et al., 2021).

These empirical observations raise immediate questions: (1) What properties of MSAs do we need to better optimize NNs? Do the long-range dependencies of MSAs help NNs learn? (2) Do MSAs act like Convs? If not, how are they different? (3) How can we harmonize MSAs with Convs? Can we just leverage their advantages?

We provide an explanation of how MSAs work by addressing them as a trainable spatial smoothing of feature maps, because Eq. (1) also suggests that MSAs average feature map values with positive importance-weights. Even non-trainable spatial smoothings, such as a small 2×2 box blur, help CNNs see better (Zhang, 2019; Anonymous, 2022). These simple spatial smoothings not only improve accuracy but also robustness by ensembling feature map points and flattening the loss landscapes (Anonymous, 2022). Surprisingly, spatial smoothings have the properties of MSAs (1) – (3). See Appendix B for more detailed discussions on the similarities between spatial smoothing and MSAs.

1.2 Contribution

We address the three key questions:

(1) **What properties of MSAs do we need to improve optimization?** We present empirical evidences to support that MSA is generalized spatial smoothing. It means that MSAs improve performance because their formulation—Eq. (1)—is an appropriate inductive bias. Their weak inductive bias disrupts NN training. In particular, *a key feature of MSAs is their data specificity*, not long-range dependency. As an extreme example, local MSAs with a 3×3 receptive field outperforms global MSA because they reduce unnecessary degrees of freedom.

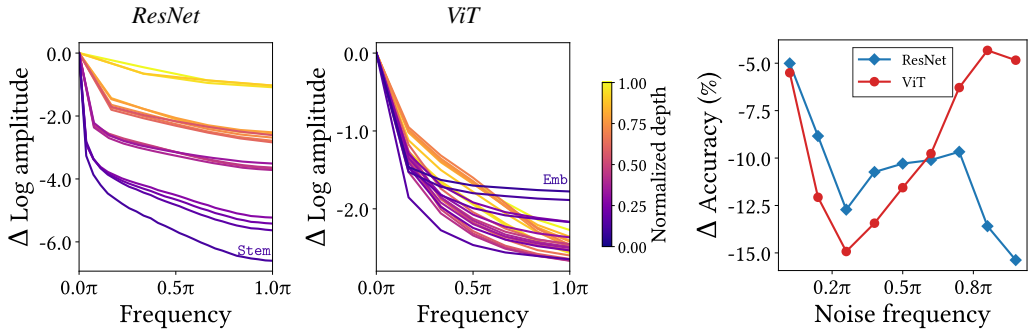

(a) Relative log amplitudes of Fourier transformed feature maps. (b) Robustness for noise frequency

Figure 2: **The Fourier analysis shows that MSAs do not act like Convs**. *Left*: Relative log amplitudes of Fourier transformed feature map show that ViT tends to reduce high-frequency signals, while ResNet amplifies them. Δ Log amplitude is the difference between the log amplitude at frequency 0.0π (center) and at 1.0π (boundary). See Fig. 8 for more detailed analysis. *Right*: We measure the decrease in accuracy against frequency-based random noise. ResNet is vulnerable to high-frequency noise, while ViT is robust against them. We use frequency window size of 0.1π.

How do MSAs improve performance? MSAs have their advantages and disadvantages. On the one hand, they flatten loss landscapes as shown in Fig. 1. The flatter the loss landscape, the better the performance and generalization (Li et al., 2018; Keskar et al., 2016; Santurkar et al., 2018; Foret et al., 2020; Chen et al., 2021). Thus, they improve not only accuracy but also robustness in large data regimes. On the other hand, MSAs allow negative Hessian eigenvalues in small data regimes. This means that the loss landscapes of MSAs are non-convex, and this non-convexity disturbs NN optimization (Dauphin et al., 2014). Large amounts of training data suppress negative eigenvalues and convexify losses.

❷ **Do MSAs act like Convs?** We show that MSAs and Convs exhibit opposite behaviors. MSAs aggregate feature maps, but Convs disperse them. Moreover, as shown in Fig. 2a, the Fourier analysis of feature maps shows that MSAs reduce high-frequency signals, while Convs, conversely, amplifies high-frequency components. In other words, *MSAs are low-pass filters, but Convs are high-pass filters*. In addition, Fig. 2b indicates that Convs are vulnerable to high-frequency noise but that MSAs are not. Therefore, MSAs and Convs are complementary.

❸ **How can we harmonize MSAs with Convs?** We reveal that multi-stage NNs behave like a series connection of small independent models. Thus, applying spatial smoothing at the end of a stage improves accuracy by ensembling feature map outputs from each stage (Anonymous, 2022) as shown in Fig. 3a. Based on this finding, *we propose an alternating pattern of Convs and MSAs*. NN stages using this design pattern consists of a number of CNN blocks and one (or a few) MSA block as shown in Fig. 3c. The design pattern naturally derives the structure of canonical Transformer, which has one MLP block for one MSA block as shown in Fig. 3b. It also provides an explanation of how adding Convs to Transformer's MLP block improves accuracy and robustness (Yuan et al., 2021; Guo et al., 2021; Mao et al., 2021).

Surprisingly, models using this alternating pattern of Convs and MSAs outperform CNNs not only on large datasets but also on small datasets, such as CIFAR. This contrasts with canonical ViTs, a model that performs poorly on small amount of data. It implies that MSAs are generalized spatial smoothings that complement Convs, not simply generalized Convs.

2 What Properties of MSAs Do We Need To Improve Optimization?

To understand the underlying nature of MSAs, we investigate properties of the ViT family: e.g., vanilla ViT (Dosovitskiy et al., 2020), PiT (Heo et al., 2021), which is "ViT + multi-stage", and Swin (Liu et al., 2021), which is "ViT + multi-stage + local MSA". This section shows that these additional inductive biases help ViT learn strong representations. We also use ResNet (He et al., 2016a) for comparison. NNs are trained with DeiT-style data augmentation (Touvron et al., 2021) for 300 epochs

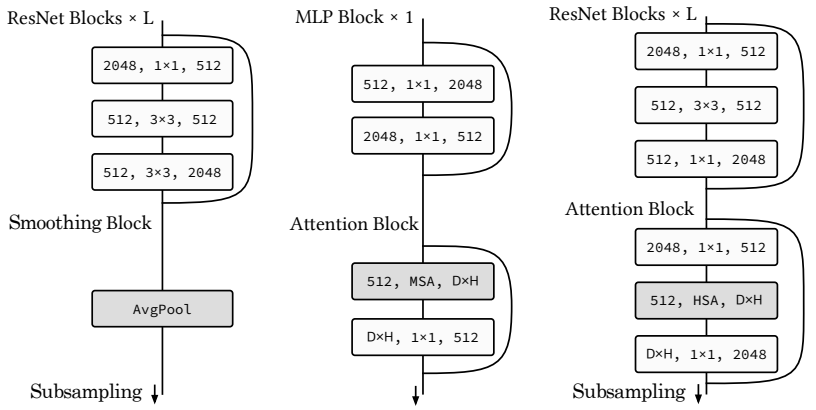

(a) Spatial smoothing (b) Canonical Transformer (c) Alternating pattern (*ours*)

Figure 3: **Comparison of three different repeating patterns**. *Left*: Spatial smoothings are located at the end of CNN stages. *Middle*: The stages of ViTs consist of repetitions of canonical Transformers. *Right*: The stages using alternating pattern consists of a number of CNN blocks and a MSA block. For more details, see Fig. 11.

from scratch. The NN training starts with gradual warmup (Goyal et al., 2017) for 5 epochs. For more detailed configurations, see Appendix A.

The stronger the inductive biases, the stronger the representations (*not regularizations*). Does the model with weak inductive bias overfit the training dataset? To address this question, we provide error of test dataset and negative log-likelihood of training dataset ($\text{NLL}_{\text{train}}$, the lower the better) on CIFAR-100, as shown in Fig. 5a.

Contrary to our expectations, the experimental result shows the stronger the inductive bias, the lower the training NLL and test error. It indicates that *ViT do not overfit the training dataset*. In addition, appropriate inductive biases, such as locality constraints for MSAs, helps NN learn strong representations. We observe the same phenomenon on CIFAR-10 and ImageNet. See Fig. C.1. Figure C.3 also supports that weak inductive bias disrupts NN training. In this experiment, small patch size for embedding hurts the predictive performance of ViT.

ViT does not overfit small training datasets. We observe that ViT does not overfit even on smaller datasets. Figure 5b presents the test error and the training NLL of ViT on subsampled datasets. In this experiment, as the size of the dataset decreases, the error increases as expected, but surprisingly, the NLL also increases. Thanks to the strong data augmentation, ViT does not overfit even on dataset of size 2%. It suggests that the poor performance of ViT in small data regimes is *not* due to overfitting.

ViT's non-convex losses lead to poor performance. How does the weak inductive bias of MSAs disturb the optimization? A loss landscape perspective provides an explanation: *the loss function of ViT is non-convex, while that of ResNet is strongly (near-)convex*. This poor loss disrupts NN training (Dauphin et al., 2014), especially in the early phase of training (Jastrzebski et al., 2021). Figure 1c and Fig. 4 provide top-5 largest Hessian eigenvalue density (Ghorbani et al., 2019; Anonymous, 2022) with batch size of 16. The figures show that ViT has a number of negative Hessian eigenvalues, while ResNet only has a few.

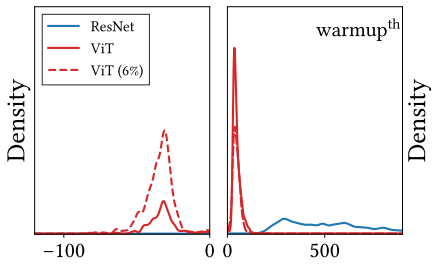

Figure 4: **Hessian max eigenvalue spectra show that MSAs have their advantages and disadvantages.** The dotted line is the spectrum of ViT using 6% dataset for training. *Left*: ViT has a number of negative Hessian eigenvalues, while ResNet only has a few. *Right*: The magnitude of ViT's positive Hessian eigenvalues is small. See Fig. 1c for more results.

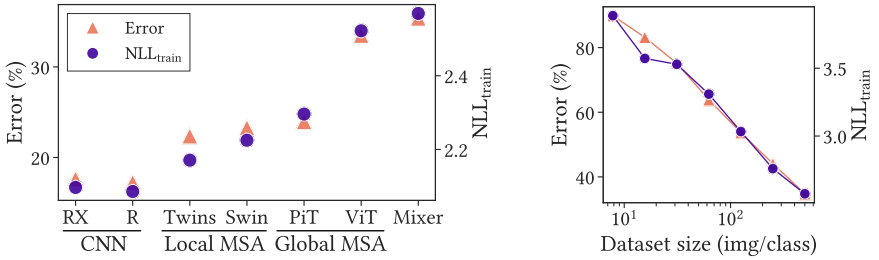

(a) Error and NLL$_{\text{train}}$ for each model. (b) Performance of ViT for dataset size.

Figure 5: **ViT does not overfit training datasets.** "R" is ResNet and "RX" is ResNeXt. *Left:* Weak inductive bias disturbs NN optimization. The lower the NLL$_{\text{train}}$, the lower the error. *Right:* The lack of dataset also disturbs NN optimization.

Figure 4 also shows that large datasets suppress negative Hessian eigenvalues in an early phase of training. Therefore, large datasets tend to help ViT learn strong representations by convexifying the loss. ResNet enjoys little benefit from large datasets because its loss is convex even on small datasets.

Loss landscape smoothing methods aids in ViT training. Loss landscape smoothing methods also can help ViT learn strong representations. In classification tasks, global average pooling (GAP) smoothens the loss landscape by strongly ensembling feature map points (Anonymous, 2022). We demonstrate how the loss smoothing method can help ViT improve the performance by analyzing ViT with GAP classifier instead of `CLS` token on CIFAR-100.

Figure 6 shows the Hessian max eigenvalue spectrum of the ViT. As expected, the result shows that GAP classifier suppresses negative Hessian max eigenvalues, suggesting that GAP convexify the loss. Since negative eigenvalues disturb NN optimization, GAP classifier improve the accuracy by $+2.7$ percent point.

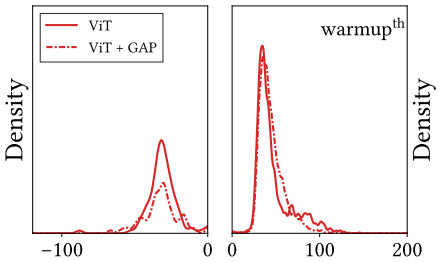

Figure 6: **GAP classifier suppresses negative Hessian max eigenvalues** in an early phase of training. We present Hessian max eigenvalue spectrum of ViT with GAP classifier instead of `CLS` token.

Likewise, Sharpness-Aware Minimization (SAM) (Foret et al., 2020), an optimizer that depends on the local smoothness of loss function, also helps NNs seek out smooth minima. Chen et al. (2021) showed that SAM improves the predictive performance of ViT.

MSAs flatten the loss landscape. Another property of MSA is that it reduces the magnitude of eigenvalues. Figure 1c and Fig. 4 shows that the eigenvalues of ViT are significantly smaller than that of CNN. While large Hessian eigenvalues impede NN training (Ghorbani et al., 2019), *MSAs can help NNs learn better representations by suppressing large Hessian eigenvalues*. Figure 1a and Fig. 1b also support the claim. In Fig. 1a, we visualize the loss landscapes by using filter normalization (Li et al., 2018). The loss landscape of ViT is flatter than that of ResNet, and this trend is noticeable at the boundary. Similarly, Fig. 1b shows that ResNet follows an irregular trajectory, especially in the early phase of training; ViT converges to the optimum along a smooth trajectory. In the large data regime, the negative Hessian eigenvalues—the disadvantage of MSA—vanishes, and only the advantage remains. As a result, ViTs outperform CNNs on large datasets, such as ImageNet and JFT (Sun et al., 2017). PiT and Swin also flatten the loss landscapes. See Fig. C.4.

The key feature of MSAs is data specificity *(not long-range dependency)*. The two distinguishing features of MSA are long-range dependency and data specificity. Contrary to popular belief, the long-range dependency hinders NN optimization. To demonstrate this, we analyze *convolutional ViT*, which consists of two-dimensional convolutional MSAs (Yang et al., 2019) instead of global MSAs. The convolutional MSA calculates self-attention only between feature map points in convolutional receptive field after unfolding the feature maps in the same way as convolution.

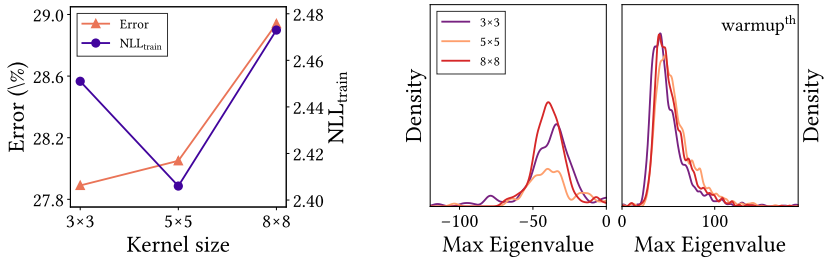

(a) Error and $\text{NLL}_{\text{train}}$ of ViT with local MSA for kernel size

(b) Hessian negative and positive max eigenvalue spectra in early phase of training

Figure 7: **Locality constraint improves the performance of ViT**. We analyze the ViT with convolutional MSAs. Convolutional MSA with 8×8 kernel is global MSA. *Left:* Local MSAs learn stronger representations than global MSA. *Right:* Locality inductive bias suppresses the negative Hessian eigenvalues, i.e., local MSAs have convex losses.

Figure 7a shows the error and $\text{NLL}_{\text{train}}$ of convolutional ViTs with kernel size of 3×3, 5×5, and 8×8 on CIFAR-100. In this experiment, 5×5 kernel outperforms 8×8 kernel—i.e., global MSA—on both the training and the test datasets. $\text{NLL}_{\text{train}}$ of 3×3 kernel is worse than that of 5×5 kernel, but better than that of global MSA. Although the test accuracies of 3×3 and 5×5 kernels are comparable, the robustness of 5×5 kernel is significantly better than that of 3×3 kernel on CIFAR-100-C (Hendrycks & Dietterich, 2019).

Figure 7b shows that the strong locality inductive bias not only reduce computational complexity as originally proposed (Liu et al., 2021), but also aid in optimization by convexifying the loss landscape. 5×5 kernel has fewer negative eigenvalues than global MSA because it restricts unnecessary degrees of freedom. 5×5 kernel also has fewer negative eigenvalues than 3×3 kernel since it ensembles a larger number of feature map points (See also Fig. 6). The amount of negative eigenvalues is minimized when the two effects are balanced.

It is clear that the data specificity improves NNs. MLP-Mixer (Tolstikhin et al., 2021; Yu et al., 2021), a model with MLP kernel that does not depend on input data, underperforms compared to ViTs. Data specificity without self-attention (Bello, 2021) improves the performance.

3 Do MSAs Act Like Convs?

Conv is data-agnostic and channel-specific. In contrast, MSA is data-specific and channel-agnostic. This section shows that these differences lead to large behavioral differences. It suggests that MSA and Conv are complementary.

MSAs are low-pass filters, but Convs are high-pass filters. As discussed in Section 1.1 and Appendix B, MSA is general form of spatial smoothings. Therefore, MSA inherits the property that spatial smoothings, e.g. blur filter, reduces high-frequency signals. Figure 8 shows the relative log amplitude (Δ log amplitude) of ViT's Fourier transformed feature map at frequency 1.0π on ImageNet. In this figure, MSAs almost always decrease the high-frequency amplitude, and MLPs—corresponding to Convs—increase the amplitude. The only exception is in the early stages of the model. In these stages, MSAs behave like Convs, i.e., they amplify the amplitude. This could be an evidence for hybrid models that use Convs in early stages and MSAs in late stages (Guo et al., 2021; Graham et al., 2021; Dai et al., 2021; Xiao et al., 2021; Srinivas et al., 2021).

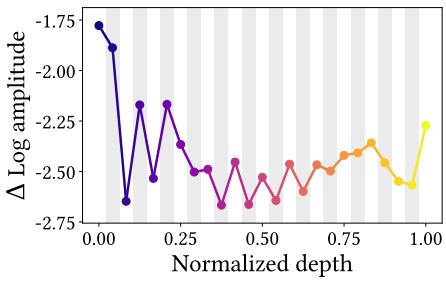

Figure 8: **MSAs (gray area) generally reduce the high-frequency component of the feature map, and MLPs (white area) amplify it**. This figure provides Δ log amplitude of ViT at 1.0π. See Fig. 2a and Fig. D.2 for more results.

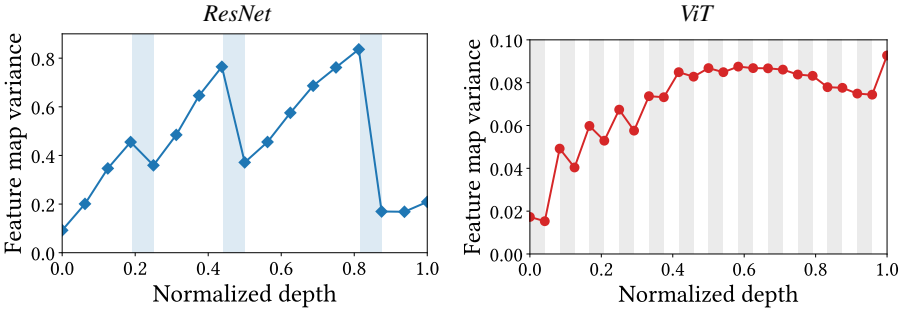

Figure 9: **MSAs (gray area) reduce the variance of feature map points, but Convs (white area) increase the variance.** The blue area is subsampling layer. The results implies that MSAs ensemble feature maps, but Convs do not.

Based on this, we can infer that *low-frequency signals and high-frequency signals are informative to MSAs and Convs, respectively*. In support of this argument, we report the robustness of ViT and ResNet against frequency-based random noise. Following Shao et al. (2021) and Anonymous (2022), we measure the decrease in accuracy with respect to data with frequency-based random noise $\boldsymbol{x}_{\text{noise}} = \boldsymbol{x}_0 + \mathcal{F}^{-1}\left(\mathcal{F}(\delta) \odot \mathbf{M}_f\right)$, where $\boldsymbol{x}_0$ is clean data, $\mathcal{F}(\cdot)$ and $\mathcal{F}^{-1}(\cdot)$ are Fourier transform and inverse Fourier transform, δ is Gaussian random noise, and $\mathbf{M}_f$ is frequency mask.

Figure 2b provides the results. As expected, it reveals that ViT and ResNet are vulnerable to low-frequency and high-frequency noise, respectively. Low-frequency signals and the high-frequency signals correspond to the shape and the texture of images. Thus, the result suggests that MSA is shape biased (Naseer et al., 2021) whereas Conv is texture biased (Geirhos et al., 2018).

MSAs aggregate feature maps, but Convs do not. As discussed in Section 1.1 and Appendix B, MSA formulation is an ensemble of feature maps. To demonstrate this claim, we measure the variance of feature map points from NN layers (Anonymous, 2022). If MSA ensembles feature maps, MSA will reduce the feature map variance.

Figure 9 shows the feature map variance of ResNet and ViT. The results demonstrate that MSAs in ViT tend to reduce the variance; conversely, Convs in ResNet and MLPs in ViT increase it. In conclusion, *MSA ensembles feature maps, but Convs do not*. As Anonymous (2022) pointed out, reducing the feature map uncertainty helps optimization by stabilizing feature maps. See Fig. D.1 for more results of PiT and Swin.

We observe two additional patterns for the feature map variance. First, the variance accumulates in every NN layer and tends to increase as the depth increases. Second, the feature map variance in ResNet peaks at the ends of the stages. Therefore, a large number of heads in the MSA at a late stage will improve performance. Furthermore, we can improve the predictive performance by inserting MSAs at the ends of the stages.

4 How Can We Harmonize MSAs With Convs?

Since MSAs and Convs are complementary, this section seeks to design a model that leverages only the advantages of the two modules. To this end, we propose design rules described in Fig. 3c, and demonstrate that the models using these rules outperforms CNNs not only in the large data regimes but also in the small data regimes, such as CIFAR.

4.1 Designing Architecture

We first investigate the properties of multi-stage NN architecture. Based on this investigation, we come to propose an alternating pattern, i.e., a principle for stacking MSAs based on CNNs.

Multi-stage NNs behave like independent models. In Fig. 9, we observe that the pattern of feature map variance repeats every stages. We find the same behavior in feature map similarity and a lesion study.

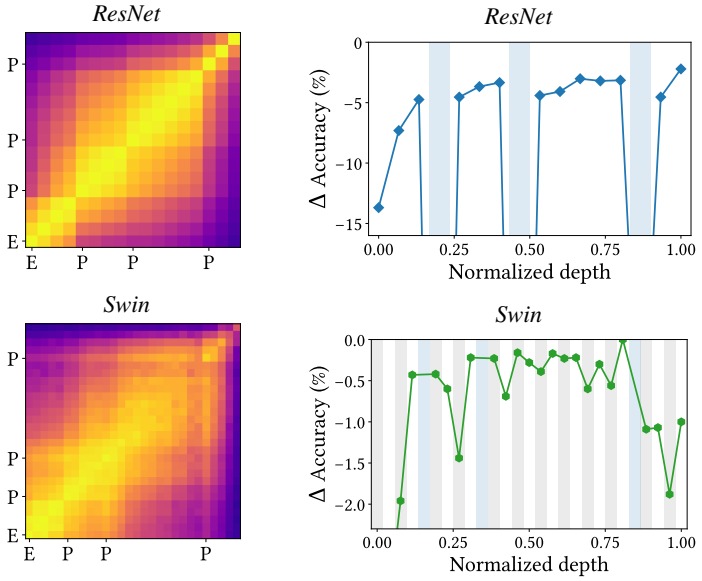

(a) Feature map similarity (b) Accuracy of one-unit-removed model.

Figure 10: **Multi-stage CNNs and ViTs behave like a series connection of small independent models.** *Left:* The feature map similarities show the block structure of ResNet and Swin. "E" stands for stem/embedding and "P" for pooling (subsampling) layer. *Right:* We measure decrease in accuracy after removing one unit from the trained model. Accuracy changes periodically, and this period is one stage. White, gray, and blue areas are Conv/MLP, MSA, and subsampling layers, respectively.

Figure 10a presents the representational similarities of ResNet and Swin on CIFAR-100. In this experiment, we use minibatch CKA (Nguyen et al., 2020) to measure the similarities. As Nguyen et al. (2020) figured out, the feature map similarity of CNNs has block structures. Likewise, we observe that feature map similarities of multi-stage ViTs, such as Swin and PiT, also have the block structures. Since vanilla ViT does not have such structure (Bhojanapalli et al., 2021; Raghu et al., 2021), this is an intrinsic characteristic of multi-stage architectures. See Fig. D.3 for more details.

Figure 10b shows the results of the lesion study (Bhojanapalli et al., 2021) that removes one NN unit from already trained ResNet and Swin during testing phase. In this experiment, we remove one 3×3 Conv layer from bottleneck block of ResNet, and one MSA or MLP block from Swin. In ResNet, removing early stage layers hurts accuracy more than removing late stage layers. More importantly, removing a layer at the early of a stage impairs accuracy more than removing a layer at an end of a stage. The case of Swin is even more interesting. In the early of a stage, removing a MLP hurts the accuracy. In the late of a stage, removing a MSA seriously impairs the accuracy. It is consistent with Fig. 8. See Fig. D.4 for the results of ViT and PiT.

Based on these findings, we expect *MSA at the end of stage* to improve predictive performance significantly. This is contrary to the popular belief that MSA at the end of the model will improve the performance (Srinivas et al., 2021; d'Ascoli et al., 2021; Graham et al., 2021; Dai et al., 2021).

Building-up rule. Considering all the insights, we propose the following design rules:

- Alternately replace Conv blocks with MSA blocks from the end of a baseline CNN model.
- If the MSA block does not improve predictive performance sufficiently, replace a Conv block with a MSA block at the end of an earlier stage.
- Use more heads and higher hidden dimensions for MSA blocks in late stages.

We call the model that follows this rule *AlterNet*. AlterNet unifies ViTs and CNNs by adjusting the ratio of MSAs and Convs as shown in Fig. 3. Figure 11 represents AlterNet based on ResNet-50 for CIFAR-100 as an example. Figure D.5 shows AlterNet for ImageNet.

Figure 12a shows the accuracy of *Alter-ResNet-50*, which replaces the Conv blocks of pre-activation ResNet-50 (He et al., 2016b) with local MSAs (Liu et al., 2021) according to the rules, on CIFAR-100. As we would expect, MSAs in the last stage (`c4`) significantly improve the accuracy. Surprisingly, a MSA in 2nd stage (`c2`) improve the accuracy, while two or more MSAs in the 3rd stage (`c3`) reduce it. In conclusion, MSAs in the late of the stages play an important role in prediction.

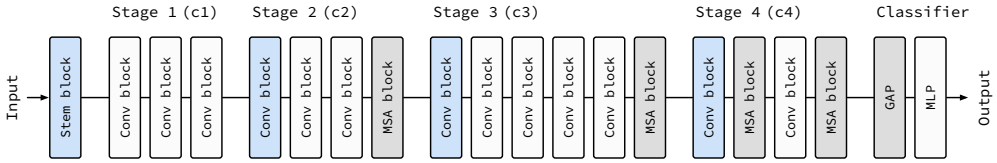

Figure 11: **Detailed architecture of Alter-ResNet-50 for CIFAR-100.** Alter-ResNet-50 is based on pre-activation ResNet-50. White, gray, and blue blocks mean Conv, MSA, and subsampling blocks. Following Swin, MSAs in stages 1 to 4 use 3, 6, 12, and 24 heads, respectively.

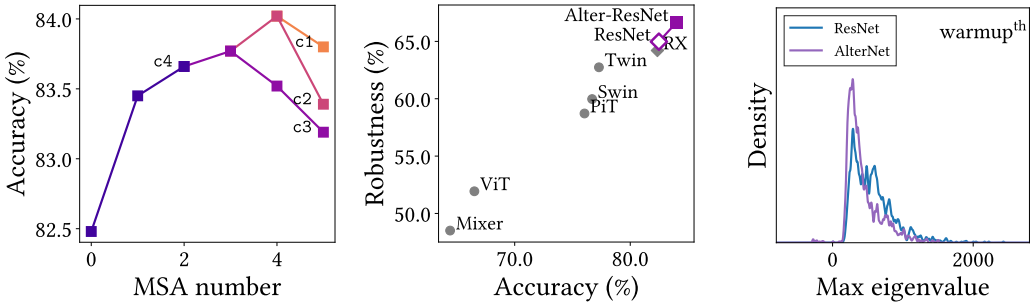

(a) Accuracy of AlterNet for MSA number

(b) Accuracy and robustness in a small data regime (CIFAR-100)

(c) Hessian max eigenvalue spectra in an early phase of training

Figure 12: **Models with an alternating pattern of Convs and MSAs outperform CNNs and ViTs.** *Left:* MSAs in the late of the stages improve accuracy. We replace Convs of ResNet with MSAs one by one according to the building-up rules. `c1` to `c4` stands for the stages. Several MSAs in `c3` harm the accuracy, but the MSA at the end of `c2` improves it. *Center:* AlterNet outperforms CNNs even in a small data regime. Robustness is mean accuracy on CIFAR-100-C. "RX" is ResNeXt. *Right:* MSAs in AlterNet suppress the large eigenvalues; i.e., AlterNet has a flatter loss landscape than ResNet in the early phase of training.

Figure 12c demonstrates that MSAs suppress large eigenvalues while allowing only a few negative eigenvalues. As explained in Section 3, large datasets compensate for the shortcoming of MSAs. Therefore, more data allows more MSA for models.

4.2 Performance

Figure 12b shows accuracy and corruption robustness of Alter-ResNet-50 and other baselines on CIFAR-100 and CIFAR-100-C. Since CIFAR is a small dataset, CNNs outperforms conventional ViTs. Surprisingly, Alter-ResNet, the model with MSAs following the appropriate building-up rule, outperforms CNNs even in the small data regime. It suggests that MSAs complement Convs. In the same manner, this simple modification shows competitive performance on larger datasets, such as ImageNet. See Fig. E.1 for mode details.

5 Discussion

The present work demonstrates that MSA is not simply generalized Conv, but rather generalized spatial smoothing that complements Conv. MSA helps NN learn strong representations by ensembling feature map points and flattening the loss landscape. Since the main objective of this work is to investigate the nature of MSA for computer vision, we preserve the architectures of Conv and MSA blocks in AlterNet. Thus, AlterNet has a strong potential for future improvements. In addition, AlterNet can conveniently replace the backbone for other vision tasks such as dense prediction (Carion et al., 2020). As Anonymous (2022) pointed out, global average pooling (GAP) for simple classification tasks has a strong tendency to ensemble feature maps, but NNs for dense prediction do not use GAP. Therefore, we believe that MSA to be able to significantly improve the results in dense prediction tasks by ensembling feature maps. Lastly, strong data augmentation for MSA training harms uncertainty calibration as shown in Fig. F.1a. We leave a detailed investigation for future work.

REFERENCES

Anonymous. Blurs make results clearer: Spatial smoothings to improve accuracy, uncertainty, and robustness. In *Submitted to The Tenth International Conference on Learning Representations*, 2022. URL https://openreview.net/forum?id=34mWBCWMxh9. under review.

Irwan Bello. Lambdanetworks: Modeling long-range interactions without attention. *arXiv preprint arXiv:2102.08602*, 2021.

Srinadh Bhojanapalli, Ayan Chakrabarti, Daniel Glasner, Daliang Li, Thomas Unterthiner, and Andreas Veit. Understanding robustness of transformers for image classification. *arXiv preprint arXiv:2103.14586*, 2021.

Nicolas Carion, Francisco Massa, Gabriel Synnaeve, Nicolas Usunier, Alexander Kirillov, and Sergey Zagoruyko. End-to-end object detection with transformers. In *European Conference on Computer Vision*, pp. 213–229. Springer, 2020.

Xiangning Chen, Cho-Jui Hsieh, and Boqing Gong. When vision transformers outperform resnets without pretraining or strong data augmentations. *arXiv preprint arXiv:2106.01548*, 2021.

Xiangxiang Chu, Zhi Tian, Yuqing Wang, Bo Zhang, Haibing Ren, Xiaolin Wei, Huaxia Xia, and Chunhua Shen. Twins: Revisiting the design of spatial attention in vision transformers. *arXiv preprint arXiv:2104.13840*, 1(2):3, 2021.

Jean-Baptiste Cordonnier, Andreas Loukas, and Martin Jaggi. On the relationship between self-attention and convolutional layers. *arXiv preprint arXiv:1911.03584*, 2019.

Ekin D Cubuk, Barret Zoph, Jonathon Shlens, and Quoc V Le. Randaugment: Practical automated data augmentation with a reduced search space. In *Proceedings of the IEEE/CVF Conference on Computer Vision and Pattern Recognition Workshops*, pp. 702–703, 2020.

Zihang Dai, Hanxiao Liu, Quoc V Le, and Mingxing Tan. Coatnet: Marrying convolution and attention for all data sizes. *arXiv preprint arXiv:2106.04803*, 2021.

Stéphane d'Ascoli, Hugo Touvron, Matthew Leavitt, Ari Morcos, Giulio Biroli, and Levent Sagun. Convit: Improving vision transformers with soft convolutional inductive biases. *arXiv preprint arXiv:2103.10697*, 2021.

Yann Dauphin, Razvan Pascanu, Caglar Gulcehre, Kyunghyun Cho, Surya Ganguli, and Yoshua Bengio. Identifying and attacking the saddle point problem in high-dimensional non-convex optimization. *arXiv preprint arXiv:1406.2572*, 2014.

Alexey Dosovitskiy, Lucas Beyer, Alexander Kolesnikov, Dirk Weissenborn, Xiaohua Zhai, Thomas Unterthiner, Mostafa Dehghani, Matthias Minderer, Georg Heigold, Sylvain Gelly, et al. An image is worth 16x16 words: Transformers for image recognition at scale. *arXiv preprint arXiv:2010.11929*, 2020.

Pierre Foret, Ariel Kleiner, Hossein Mobahi, and Behnam Neyshabur. Sharpness-aware minimization for efficiently improving generalization. *arXiv preprint arXiv:2010.01412*, 2020.

Robert Geirhos, Patricia Rubisch, Claudio Michaelis, Matthias Bethge, Felix A Wichmann, and Wieland Brendel. Imagenet-trained cnns are biased towards texture; increasing shape bias improves accuracy and robustness. *arXiv preprint arXiv:1811.12231*, 2018.

Behrooz Ghorbani, Shankar Krishnan, and Ying Xiao. An investigation into neural net optimization via hessian eigenvalue density. In *International Conference on Machine Learning*, pp. 2232–2241. PMLR, 2019.

Priya Goyal, Piotr Dollár, Ross Girshick, Pieter Noordhuis, Lukasz Wesolowski, Aapo Kyrola, Andrew Tulloch, Yangqing Jia, and Kaiming He. Accurate, large minibatch sgd: Training imagenet in 1 hour. *arXiv preprint arXiv:1706.02677*, 2017.

Ben Graham, Alaaeldin El-Nouby, Hugo Touvron, Pierre Stock, Armand Joulin, Hervé Jégou, and Matthijs Douze. Levit: a vision transformer in convnet's clothing for faster inference. *arXiv preprint arXiv:2104.01136*, 2021.

Jianyuan Guo, Kai Han, Han Wu, Chang Xu, Yehui Tang, Chunjing Xu, and Yunhe Wang. Cmt: Convolutional neural networks meet vision transformers. *arXiv preprint arXiv:2107.06263*, 2021.

Kaiming He, Xiangyu Zhang, Shaoqing Ren, and Jian Sun. Deep residual learning for image recognition. In *Proceedings of the IEEE conference on computer vision and pattern recognition*, pp. 770–778, 2016a.

Kaiming He, Xiangyu Zhang, Shaoqing Ren, and Jian Sun. Identity mappings in deep residual networks. In *European conference on computer vision*, pp. 630–645. Springer, 2016b.

Dan Hendrycks and Thomas Dietterich. Benchmarking neural network robustness to common corruptions and perturbations. *Proceedings of the International Conference on Learning Representations*, 2019.

Byeongho Heo, Sangdoo Yun, Dongyoon Han, Sanghyuk Chun, Junsuk Choe, and Seong Joon Oh. Rethinking spatial dimensions of vision transformers. *arXiv preprint arXiv:2103.16302*, 2021.

Jiri Hron, Yasaman Bahri, Jascha Sohl-Dickstein, and Roman Novak. Infinite attention: Nngp and ntk for deep attention networks. In *International Conference on Machine Learning*, pp. 4376–4386. PMLR, 2020.

Gao Huang, Yu Sun, Zhuang Liu, Daniel Sedra, and Kilian Q Weinberger. Deep networks with stochastic depth. In *European conference on computer vision*, pp. 646–661. Springer, 2016.

Stanislaw Jastrzebski, Devansh Arpit, Oliver Astrand, Giancarlo B Kerg, Huan Wang, Caiming Xiong, Richard Socher, Kyunghyun Cho, and Krzysztof J Geras. Catastrophic fisher explosion: Early phase fisher matrix impacts generalization. In *International Conference on Machine Learning*, pp. 4772–4784. PMLR, 2021.

Nitish Shirish Keskar, Dheevatsa Mudigere, Jorge Nocedal, Mikhail Smelyanskiy, and Ping Tak Peter Tang. On large-batch training for deep learning: Generalization gap and sharp minima. *arXiv preprint arXiv:1609.04836*, 2016.

Alex Krizhevsky, Geoffrey Hinton, et al. Learning multiple layers of features from tiny images. 2009.

Hao Li, Zheng Xu, Gavin Taylor, Christoph Studer, and Tom Goldstein. Visualizing the loss landscape of neural nets. *Advances in Neural Information Processing Systems*, 31, 2018.

Ze Liu, Yutong Lin, Yue Cao, Han Hu, Yixuan Wei, Zheng Zhang, Stephen Lin, and Baining Guo. Swin transformer: Hierarchical vision transformer using shifted windows. *arXiv preprint arXiv:2103.14030*, 2021.

Ilya Loshchilov and Frank Hutter. Sgdr: Stochastic gradient descent with warm restarts. *arXiv preprint arXiv:1608.03983*, 2016.

Ilya Loshchilov and Frank Hutter. Decoupled weight decay regularization. In *International Conference on Learning Representations*, 2018.

Xiaofeng Mao, Gege Qi, Yuefeng Chen, Xiaodan Li, Shaokai Ye, Yuan He, and Hui Xue. Rethinking the design principles of robust vision transformer. *arXiv preprint arXiv:2105.07926*, 2021.

Matthias Minderer, Josip Djolonga, Rob Romijnders, Frances Hubis, Xiaohua Zhai, Neil Houlsby, Dustin Tran, and Mario Lucic. Revisiting the calibration of modern neural networks. *arXiv preprint arXiv:2106.07998*, 2021.

Muzammal Naseer, Kanchana Ranasinghe, Salman Khan, Munawar Hayat, Fahad Shahbaz Khan, and Ming-Hsuan Yang. Intriguing properties of vision transformers. *arXiv preprint arXiv:2105.10497*, 2021.

Thao Nguyen, Maithra Raghu, and Simon Kornblith. Do wide and deep networks learn the same things? uncovering how neural network representations vary with width and depth. *arXiv preprint arXiv:2010.15327*, 2020.

Namuk Park, Taekyu Lee, and Songkuk Kim. Vector quantized bayesian neural network inference for data streams. In *Proceedings of the AAAI Conference on Artificial Intelligence*, volume 35, pp. 9322–9330, 2021.

Adam Paszke, Sam Gross, Francisco Massa, Adam Lerer, James Bradbury, Gregory Chanan, Trevor Killeen, Zeming Lin, Natalia Gimelshein, Luca Antiga, et al. Pytorch: An imperative style, high-performance deep learning library. *Advances in neural information processing systems*, 32: 8026–8037, 2019.

Sayak Paul and Pin-Yu Chen. Vision transformers are robust learners. *arXiv preprint arXiv:2105.07581*, 2021.

Maithra Raghu, Thomas Unterthiner, Simon Kornblith, Chiyuan Zhang, and Alexey Dosovitskiy. Do vision transformers see like convolutional neural networks? *arXiv preprint arXiv:2108.08810*, 2021.

Olga Russakovsky, Jia Deng, Hao Su, Jonathan Krause, Sanjeev Satheesh, Sean Ma, Zhiheng Huang, Andrej Karpathy, Aditya Khosla, Michael Bernstein, Alexander C. Berg, and Li Fei-Fei. ImageNet Large Scale Visual Recognition Challenge. *International Journal of Computer Vision (IJCV)*, 115 (3):211–252, 2015. doi: 10.1007/s11263-015-0816-y.

Shibani Santurkar, Dimitris Tsipras, Andrew Ilyas, and Aleksander Mądry. How does batch normalization help optimization? In *Proceedings of the 32nd international conference on neural information processing systems*, pp. 2488–2498, 2018.

Rulin Shao, Zhouxing Shi, Jinfeng Yi, Pin-Yu Chen, and Cho-Jui Hsieh. On the adversarial robustness of visual transformers. *arXiv preprint arXiv:2103.15670*, 2021.

Aravind Srinivas, Tsung-Yi Lin, Niki Parmar, Jonathon Shlens, Pieter Abbeel, and Ashish Vaswani. Bottleneck transformers for visual recognition. In *Proceedings of the IEEE/CVF Conference on Computer Vision and Pattern Recognition*, pp. 16519–16529, 2021.

Chen Sun, Abhinav Shrivastava, Saurabh Singh, and Abhinav Gupta. Revisiting unreasonable effectiveness of data in deep learning era. In *Proceedings of the IEEE international conference on computer vision*, pp. 843–852, 2017.

Christian Szegedy, Vincent Vanhoucke, Sergey Ioffe, Jon Shlens, and Zbigniew Wojna. Rethinking the inception architecture for computer vision. In *Proceedings of the IEEE conference on computer vision and pattern recognition*, pp. 2818–2826, 2016.

Ilya Tolstikhin, Neil Houlsby, Alexander Kolesnikov, Lucas Beyer, Xiaohua Zhai, Thomas Unterthiner, Jessica Yung, Daniel Keysers, Jakob Uszkoreit, Mario Lucic, et al. Mlp-mixer: An all-mlp architecture for vision. *arXiv preprint arXiv:2105.01601*, 2021.

Hugo Touvron, Matthieu Cord, Matthijs Douze, Francisco Massa, Alexandre Sablayrolles, and Hervé Jégou. Training data-efficient image transformers & distillation through attention. In *International Conference on Machine Learning*, pp. 10347–10357. PMLR, 2021.

Shikhar Tuli, Ishita Dasgupta, Erin Grant, and Thomas L Griffiths. Are convolutional neural networks or transformers more like human vision? *arXiv preprint arXiv:2105.07197*, 2021.

Ashish Vaswani, Noam Shazeer, Niki Parmar, Jakob Uszkoreit, Llion Jones, Aidan N Gomez, Łukasz Kaiser, and Illia Polosukhin. Attention is all you need. In *Advances in neural information processing systems*, pp. 5998–6008, 2017.

Phil Wang. Implementation of vision transformer. https://github.com/lucidrains/vit-pytorch, 2021.

Yeming Wen, Ghassen Jerfel, Rafael Muller, Michael W Dusenberry, Jasper Snoek, Balaji Lakshminarayanan, and Dustin Tran. Combining ensembles and data augmentation can harm your calibration. In *International Conference on Learning Representations*, 2021.

Ross Wightman. Pytorch image models. https://github.com/rwightman/pytorch-image-models, 2019.

Tete Xiao, Mannat Singh, Eric Mintun, Trevor Darrell, Piotr Dollár, and Ross Girshick. Early convolutions help transformers see better. *arXiv preprint arXiv:2106.14881*, 2021.

Saining Xie, Ross Girshick, Piotr Dollár, Zhuowen Tu, and Kaiming He. Aggregated residual transformations for deep neural networks. In *Proceedings of the IEEE conference on computer vision and pattern recognition*, pp. 1492–1500, 2017.

Weijian Xu, Yifan Xu, Tyler Chang, and Zhuowen Tu. Co-scale conv-attentional image transformers, 2021.

Baosong Yang, Longyue Wang, Derek F Wong, Lidia S Chao, and Zhaopeng Tu. Convolutional self-attention networks. In *Proceedings of the 2019 Conference of the North American Chapter of the Association for Computational Linguistics: Human Language Technologies, Volume 1 (Long and Short Papers)*, pp. 4040–4045, 2019.

Zhewei Yao, Amir Gholami, Kurt Keutzer, and Michael W Mahoney. Pyhessian: Neural networks through the lens of the hessian. In *2020 IEEE International Conference on Big Data (Big Data)*, pp. 581–590. IEEE, 2020.

Tan Yu, Xu Li, Yunfeng Cai, Mingming Sun, and Ping Li. Rethinking token-mixing mlp for mlp-based vision backbone. *arXiv preprint arXiv:2106.14882*, 2021.

Kun Yuan, Shaopeng Guo, Ziwei Liu, Aojun Zhou, Fengwei Yu, and Wei Wu. Incorporating convolution designs into visual transformers. *arXiv preprint arXiv:2103.11816*, 2021.

Sangdoo Yun, Dongyoon Han, Seong Joon Oh, Sanghyuk Chun, Junsuk Choe, and Youngjoon Yoo. Cutmix: Regularization strategy to train strong classifiers with localizable features. In *Proceedings of the IEEE/CVF International Conference on Computer Vision*, pp. 6023–6032, 2019.

Hongyi Zhang, Moustapha Cisse, Yann N Dauphin, and David Lopez-Paz. mixup: Beyond empirical risk minimization. In *International Conference on Learning Representations*, 2018.

Richard Zhang. Making convolutional networks shift-invariant again. In *International conference on machine learning*, pp. 7324–7334. PMLR, 2019.

Zhun Zhong, Liang Zheng, Guoliang Kang, Shaozi Li, and Yi Yang. Random erasing data augmentation. In *Proceedings of the AAAI Conference on Artificial Intelligence*, volume 34, pp. 13001–13008, 2020.

A Experimental Setup

We obtain the main experimental results with two kind of machines for CIFAR (Krizhevsky et al., 2009). The first one is the Intel Xeon W-2123 Processor, 32GB memory, and a single GeForce RTX 2080 Ti, and the other is four Intel Intel Broadwell CPUs, 15GB memory, and a single NVIDIA T4. For ImageNet (Russakovsky et al., 2015), we use AMD Ryzen Threadripper 3960X 24-Core Processor, 256GB memory, and four GeForce RTX 2080 Ti. Models are implemented in PyTorch (Paszke et al., 2019).

NNs are trained using categorical cross-entropy (NLL) loss and AdamW optimizer (Loshchilov & Hutter, 2018) with initial learning rate of 1.25×10^{-4} and weight decay of 5×10^{-2}. We also use cosine annealing scheduler (Loshchilov & Hutter, 2016). We train NNs for 300 epochs with batch size of 96 on CIFAR, and with batch size of 128 on ImageNet. We start training with gradual warmup (Goyal et al., 2017) for 5 epochs. Following Touvron et al. (2021), strong data augmentations, such as RandAugment (Cubuk et al., 2020), Random Erasing (Zhong et al., 2020), label smoothing (Szegedy et al., 2016), mixup (Zhang et al., 2018), and CutMix (Yun et al., 2019), are used for training. Stochastic depth (Huang et al., 2016) is also used to regularize NNs. See source code for detailed configurations.

We mainly report the performances of ResNet-50, ViT-Ti, PiT-Ti, and Swin-Ti. Their training throughputs on CIFAR-100 are 320, 434, 364, and 469 image/sec respectively, which are comparable to each other. In Figs. 5a and C.1a, we also report the predictive performance of ResNeXt-50 (Xie et al., 2017), Twins-S (Chu et al., 2021), and MLP-Mixer-Ti (Tolstikhin et al., 2021). In Fig. E.1, we additionally report the predictive performance of ConViT-Ti (d'Ascoli et al., 2021), LeViT-128S (Graham et al., 2021), CoaT-Lite-Ti (Xu et al., 2021), and MLP-Mixer-B (Tolstikhin et al., 2021). We use patch size of 2×2 for ViT and PiT on CIFAR. For Swin, we use patch size of 1×1 and window size of 4×4. We use patch size of 4×4 for ViT only in Fig. 7.

All models for CIFAR, and ResNet, ViT, and AlterNet for ImageNet are trained from scratch. We use pertained PiT and Swin from Wightman (2019) for ImageNet. The implementations of Vision Transformers are based on Wightman (2019) and Wang (2021).

For Hessian max eigenvalue spectrum, we use power iteration with batch size of 16 to produce the top-5 greatest eigenvalues. To this end, Yao et al. (2020)'s implementation is used. We modify the algorithm to calculate the eigenvalues with respect to ℓ_2 regularized NLL on augmented training dataset. In the strict sense, the weight decay is not ℓ_2 regularization, but we neglect the difference.

B Similarities Between Spatial Smoothings and MSAs

As mentioned in Section 1.1, spatial smoothings before subsampling layers help CNNs see better (Zhang, 2019; Anonymous, 2022). Anonymous (2022) showed that such improvement in performance is possible due to (Bayesian) feature map ensembles. To this end, they used *data-complemented Bayesian NN (BNN)* (Park et al., 2021):

$$p(\boldsymbol{z}_j|\boldsymbol{x}_j, \mathcal{D}) \simeq \sum_i \pi(\boldsymbol{x}_i|\boldsymbol{x}_j)\, p(\boldsymbol{z}_j|\boldsymbol{x}_i, \boldsymbol{w}_i) \tag{2}$$

where $\pi(\boldsymbol{x}_i|\boldsymbol{x}_j)$ is normalized importance weight of a feature map point $\boldsymbol{x}_i$ with respect to another feature map $\boldsymbol{x}_j$, i.e., $\sum_i \pi(\boldsymbol{x}_i|\boldsymbol{x}_j) = 1$. The importance is defined as a similarity between $\boldsymbol{x}_i$ and $\boldsymbol{x}_j$. $p(\boldsymbol{z}_j|\boldsymbol{x}_i, \boldsymbol{w}_i)$ and $p(\boldsymbol{z}_j|\boldsymbol{x}_j, \mathcal{D})$ are one NN prediction and output predictive distribution, respectively. $\boldsymbol{w}_i$ is a NN weight sample from posterior $p(\boldsymbol{w}|\mathcal{D})$ with respect to training dataset $\mathcal{D}$. Put shortly, Eq. (2) complements a prediction with other predictions based on similarities. For instance, a 2×2 box blur ensembles four neighboring feature map points, each with ¼ of the same importance.

We note that the formulations for self-attention and data-complemented BNN are identical. The `Softmax` term and $\boldsymbol{V}$ in Eq. (1) exactly correspond to $\pi(\boldsymbol{x}_i|\boldsymbol{x}_j)$ and $p(\boldsymbol{z}_j|\boldsymbol{x}_i, \boldsymbol{w}_i)$ in Eq. (2). The weight samples in Eq. (2) is correspond to the multi-heads of MSAs (cf. (Hron et al., 2020)).

Likewise, the properties of spatial smoothing are the same as those of MSAs (Anonymous, 2022): (1) Spatial smoothing improves the accuracy of CNNs. In addition, spatial smoothing predicts well-calibrated uncertainty. (2) Spatial smoothing is robust against MC dropout (which is equivalent

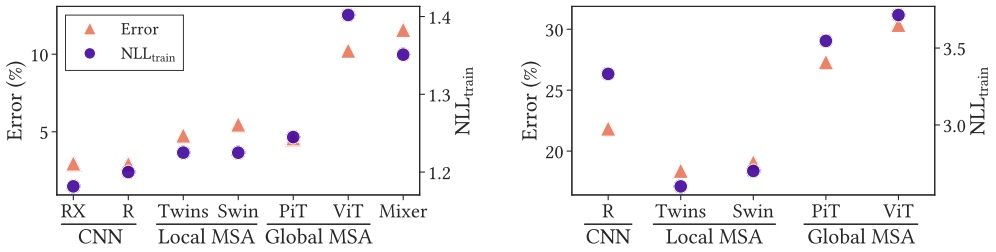

(a) CIFAR-10 (b) ImageNet

Figure C.1: **The lower the training NLL, the lower the test error.** "R" is ResNet and "RX" is ResNeXt. *Left:* In small data regimes, such as CIFAR-10 and CIFAR-100 (Fig. 5a), the cons of MSAs outweigh the pros, i.e., the non-convex losses disturb ViT optimization. *Right:* Large datasets convexify the loss functions. Therefore, the pros of MSAs outweigh the cons in large data regimes, i.e., MSAs help NN learn strong representations by flattening the loss landscapes.

to image occlusion), data corruption, and adversarial attacks, and particularly robust against high-frequency noise. (3) Spatial smoothing layers closer to the output layer significantly improves the predictive performance.

Taking all these observations together, *we provide an explanation of how MSAs work by addressing them as a general form of spatial smoothing or an implementation of data-complemented BNN.* Spatial smoothing improves performance in the following ways (Anonymous, 2022): (1) Spatial smoothing helps in NN optimization by flattening the loss landscapes. Even a small 2×2 blur filter significantly improves performance. (2) Spatial smoothing is a low-pass filter. CNNs are vulnerable to high-frequency noise, but spatial smoothing improves the robustness against it by reducing high-frequency noise effectively. (3) Spatial smoothing is effective when applied at the end of a stage because it aggregates all the feature maps that are transformed in various ways. The main paper shows that these mechanisms are maintained for MSAs.

C ViTs From a Loss Landscape Perspective

This section provides further explanations of the analysis in Section 2.

The lower the NLL on training dataset, the lower the error on test dataset. Figure 5a demonstrates that low training NLL results in low test error on CIFAR-100. We observe the same pattern on CIFAR-10 and ImageNet. Figure C.1 shows the result.

In small data regimes, such as CIFAR-10 (Fig. C.1a) and CIFAR-100 (Fig. 5a), both the error and the NLL$_{\text{train}}$ of ViTs are inferior to those of CNNs. It suggests that the cons of MSA outweigh the pros. As discussed in Fig. 4, ViTs suffers from the non-convex losses, and the non-convex loss disturb ViT optimization.

In large data regimes, such as ImageNet (Fig. C.1b), both the error and the NLL$_{\text{train}}$ of ViTs with local MSAs are superior to those of CNNs. Since large datasets convexify the loss function as discussed in Fig. 4, the pros of MSAs outweigh the cons. Therefore, MSAs help NNs learn strong representations by flattening the loss landscapes.

Rigorous discussion on regularization of CNN's inductive bias. In Fig. 5a, we compare ResNet-50 and ViT-Ti, which are comparable models in terms of throughput. Through the comparison, we argue that a weak inductive bias hinders NN training, and CNN's inductive biases—Conv's inductive bias and multi-stage architecture—help NN learn strong representations.

It is generally true; but the inductive biases of CNN somewhat regularizes NNs. We analyze two comparable models in terms of NLL$_{\text{train}}$ on CIFAR-100. The NLL$_{\text{train}}$ of ResNet-18, a model smaller than ResNet-50, is 2.31 and the error is 22.0%. The NLL$_{\text{train}}$ of ViT-S, a larger than ViT-Ti, is 2.17 and the error is 30.4%. In summary, the inductive biases of CNNs improve accuracy for similar training NLL.

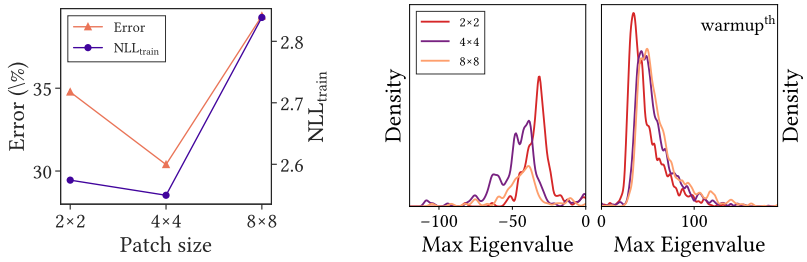

(a) Error and $\text{NLL}_{\text{train}}$ of ViT for patch size

(b) Negative and positive Hessian max eigenvalue spectra in early phase of training

Figure C.3: **A small patch size does not guarantee better performance**. We analyze ViTs with three embedded patch sizes: 2×2, 4×4, and 8×8. Note that every MSAs have global receptive fields. *Left:* A large size of patch harms the performance as we would expect, and surprisingly, a small size of patch also harms it. *Right:* A small patch size, or weak inductive bias, allows the negative eigenvalues. This is another evidence that weak inductive bias hinders NN optimization. On the other hand, MSA with a small patch size reduces the magnitude of eigenvalues because it ensembles a large number of feature map points. The performance is optimized when these two effects are balanced.

Most of the improvement come from multi-stage architecture, not the inductive bias of Conv. The $\text{NLL}_{\text{train}}$ of the PiT-Ti, multi-stage ViT-Ti, is 2.29 and the error is 24.1 %. The accuracy of PiT is only 1.9 percent point lower than that of ResNet.

ViT does not overfit small training dataset even with a large number of epochs. Figure 5b shows that ViT does not overfit small training datasets such as CIFAR. We observe the same phenomenon in ViT training with a large number of epochs.

In Fig. C.2, we train ViT and ResNet for 75, 150, 300, 600, and 1200 epochs. The experimental results show that the $\text{NLL}_{\text{train}}$ and the error decrease as the epoch increases. However, the predictive performances of ViT is inferior to those of ResNet across a whole range of epochs.

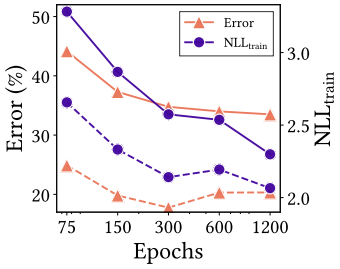

Figure C.2: **A large number of epochs does not make ViT overfit the training dataset of CIFAR**. Solid line is the predictive performance of ViT and dashed line is that of ResNet.

A smaller patch size does not always imply better results. ViT splits the image into multiple patches. The smaller the patch size, the greater the flexibility of expression and the weaker the inductive bias. By analyzing ViT with three patch sizes—2×2, 4×4, and 8×8—we again demonstrate that weak inductive bias disturbs NN optimization.

Figure C.3a shows the error on test dataset and NLL on the training dataset of CIFAR-100. As expected, large patch size harms the performance on both test and training datasets. Surprisingly, a small patch size also harms the performance. An appropriate patch size helps ViT learn strong representations, not regularizes ViT.

The Hessian max eigenvalue spectra in Fig. C.3b explain this observation. The results reveal that a small patch size allows negative Hessian eigenvalues. In other words, weak inductive bias makes the loss landscape non-convex. A large patch size suppresses negative eigenvalues. On the other hand, it limits the model expression and sharpens the loss landscape. The performance is optimized when these two effects are balanced.

Multi-stage architecture in PiT and local MSA in Swin also flatten the loss landscapes. As explained in Fig. 1, MSA smoothens the loss landscape. Similarly, multi-stage architecture in PiT and local MSA in Swin also help NN learn strong representations by smoothing the loss landscapes.

Figure C.4 provides loss landscape visualizations, trajectories in training phase, and Hessian eigenvalue spectra of ResNet, ViT, PiT, and Swin. Figure C.4a visualizes the global geometries of the loss functions. The loss landscape of PiT is flatter than that of ViT near the optimum. Since Swin has more

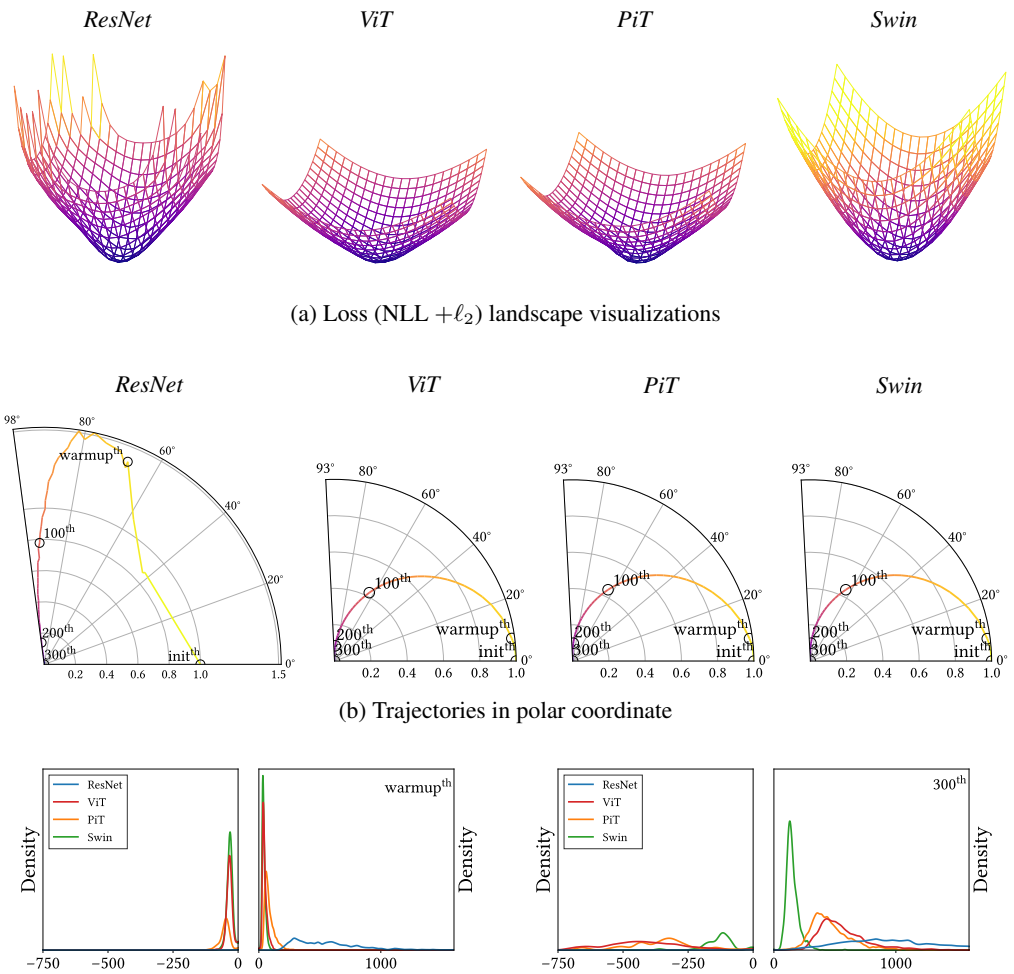

(a) Loss (NLL $+\ell_2$) landscape visualizations

(b) Trajectories in polar coordinate

(c) Negative and positive Hessian max eigenvalue spectra in early phase (*left*) and late phase (*right*) of training

Figure C.4: **Multi-stage architecture (in PiT) and local MSA (in Swin) also flatten the loss landscapes.** *Top:* PiT has a flatter loss landscape than ViT near the optimum. Swin has an almost perfect smooth parabolic loss landscape (due to ℓ_2 regularization). *Middle:* All three ViTs converge to the optima with smooth trajectories. *Bottom:* Multi-stage in PiT suppresses negative Hessian eigenvalues. Local MSA in Swin allows the negative eigenvalues, but significantly reduces the magnitude of eigenvalues.

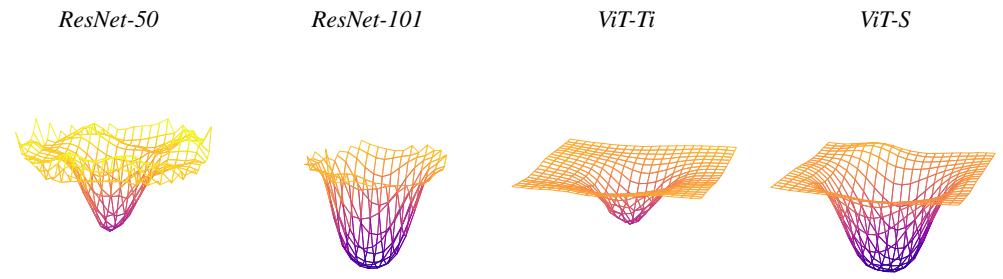

(a) NLL landscape visualizations

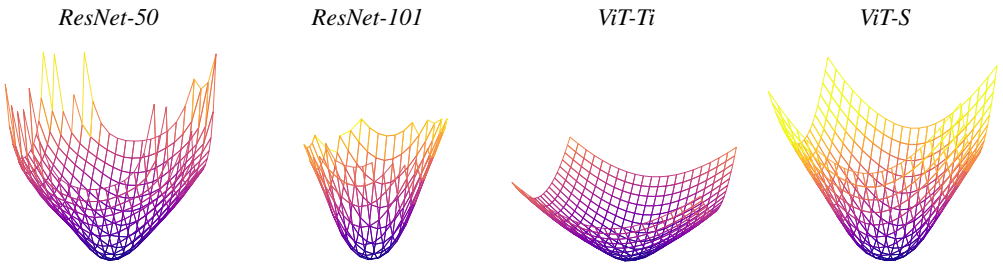

(b) Loss (NLL $+\ell_2$) landscape visualizations

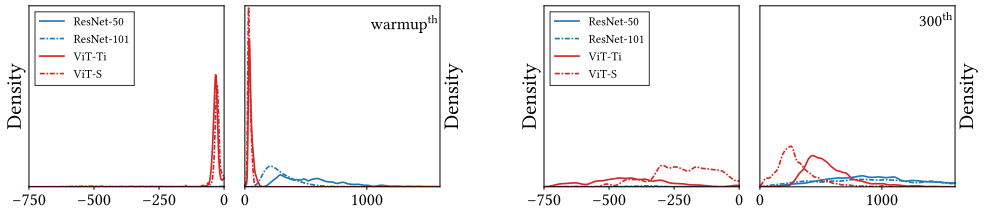

(c) Negative and positive Hessian max eigenvalue spectra in early phase (*left*) and late phase (*right*) of training

Figure C.5: **The loss landscapes of large models.** ResNet-50 and ResNet-101 are comparable to ViT-Ti and ViT-S, respectively. *Top:* Large models explore low NLLs. *Middle:* The loss landscape visualizations show that the global geometry of large models is sharp. *Bottom:* The Hessian eigenvalues of large models are smaller than that of small models. It suggests that large models have flat local geometry in early phase of training, and the flat loss helps NN learn strong representations. In late phase of training, large ViT has flat minimum while large ResNet has sharp minimum.

parameters than ViT and PiT, ℓ_2 regularization leads the loss landscape. Figure C.4b demonstrates that all the ViTs converge to the optima with smooth trajectories. These support that MSA smoothens the loss landscape. Figure C.4c shows the local geometries of the loss function by representing Hessian eigenvalues. In the early phase of training, multi-stage in PiT helps training by suppressing negative Hessian eigenvalues. Local MSA in Swin allows the negative eigenvalues, but significantly reduces the magnitude of eigenvalues. Moreover, the magnitude of Swin's Hessian eigenvalue does not significantly increases in the late phase of learning.

A large model has a flat loss in an early phase of training. Figure C.5 analyze the loss landscapes of large models, such as ResNet-101 and ViT-S. As shown in Fig. C.5a, large models explore low NLLs. These can be a surprising result, because the loss landscapes of the large model is globally sharp as shown in Fig. C.5b.

Hessian eigenvalue spectra in Fig. C.5c solve the problem: The Hessian eigenvalues of large models are smaller than that of small models in early phase of training. It indicates that large models have flat loss functions locally.

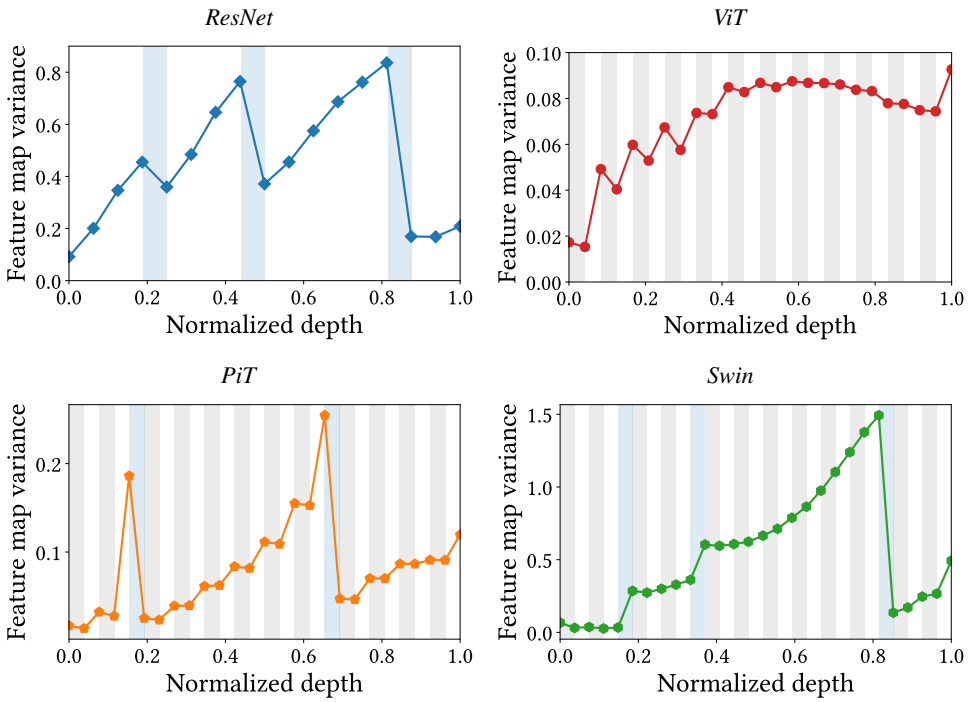

Figure D.1: **MSAs in PiT and Swin also reduce feature map variance** except in 3rd stage of Swin. White, gray, and blue areas are Conv/MLP, MSA, and subsampling layers, respectively.

D ViTs From a Feature Map Perspective

This section provides further explanations of the analysis in Section 3 and Section 4.1.

MSAs in PiT and Swin also ensemble feature maps. In Fig. 9, we show that MSAs in ViT reduce feature map variance. We observe same pattern in PiT and Swin. Figure D.1 demonstrates that MSAs in PiT and Swin also reduce the feature map variance, suggesting that they also ensemble feature maps. One exception is the 3rd stage in Swin. In the early of this stage, MSAs suppresses the increase in variance, but at the end of the stage it does not suppress it.

MSAs in PiT and Swin are also low-pass filters. As discussed in Fig. 8, MSAs in ViTs are low-pass filters, while MLPs in ViT and Convs in ResNet are high-pass filters. Likewise, we demonstrate that MSAs in PiT and Swin are also low-pass filters.

Figure D.2 shows the relative log amplitude of Fourier transformed feature maps. As in the case of ViT, MSAs in PiT and Swin generally decrease the amplitude of high-frequency signals; in contrast, MLPs increases the amplitude.

Multi-stage ViTs have the block structures. The feature map similarities of CNNs shows a block structure (Nguyen et al., 2020). As Raghu et al. (2021) figured out, ViT has uniform representations across all layers. By investigating multi-stage ViTs, we demonstrate that subsampling layers create the characteristic block structure of the representation. See Fig. D.3.

Conv in early phase of stages and MSA in late phase of stages play an important role. Figure D.4 shows the results of lesion study for ResNet and ViTs. In this experiment, we remove one 3×3 Conv layer from bottleneck block of ResNet, and one MSA or MLP block from Swin. We observe consistent results for all models: Removing Convs in early phase of stages and removing MSAs in late phase of stages significantly harm the accuracy. As a result, the accuracy varies periodically.

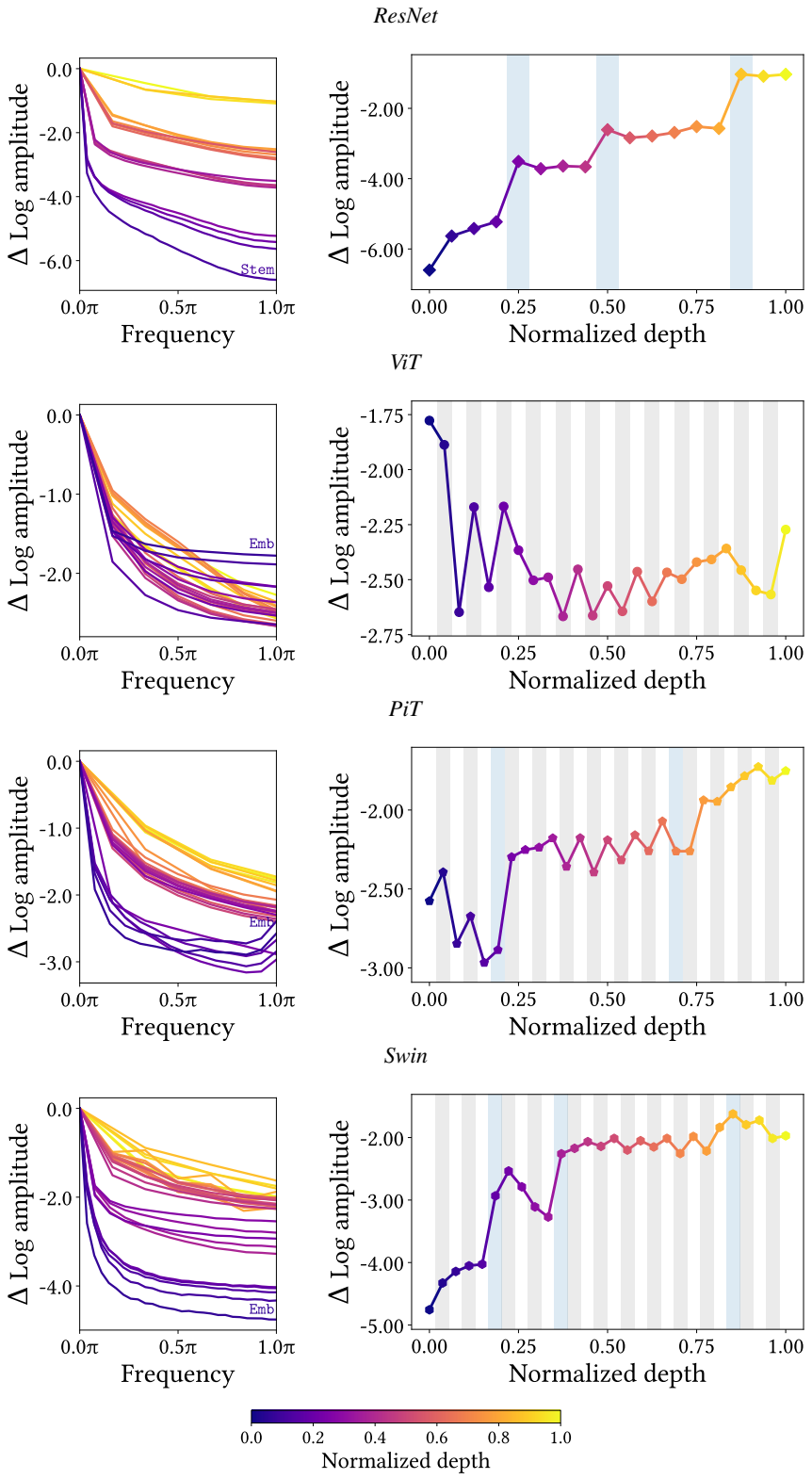

Figure D.2: **MSAs in PiT and Swin also reduce high-frequency signals**. *Left:* Δ log amplitude of Fourier transformed feature map. We only provide the diagonal components. *Right:* The high-frequency (1.0π) Δ log amplitude. White, gray, and blue areas are Conv/MLP, MSA, and subsampling layers, respectively.

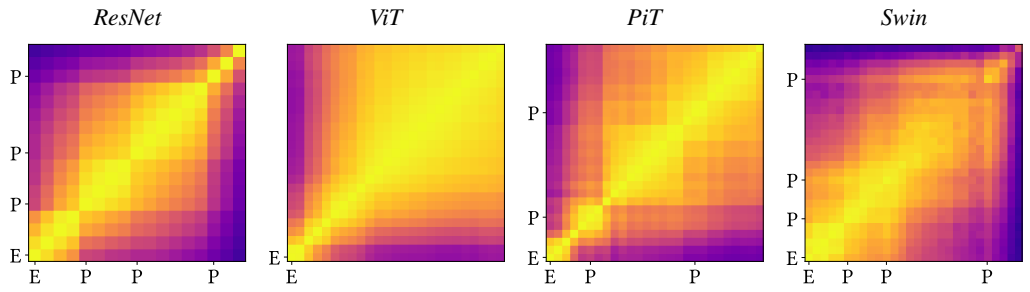

Figure D.3: **Multi-stage ViTs have block structures in representational similarities**. We observe the block structures in all multi-stage NNs, namely, ResNet, PiT, and Swin. "E" is stem/embedding and "P" is pooling (subsampling) layer.

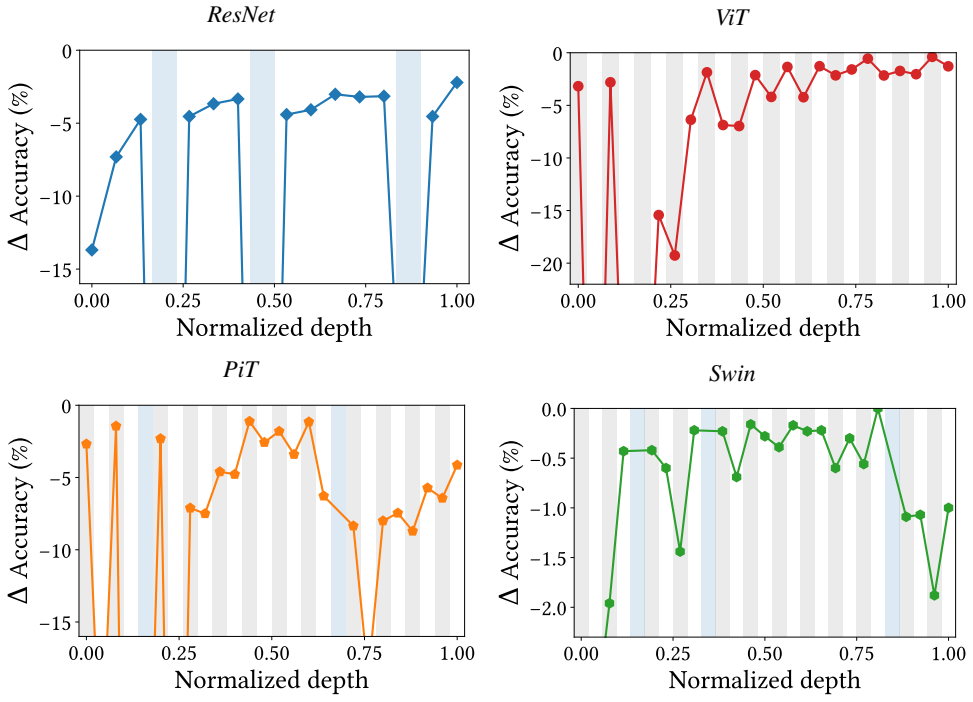

Figure D.4: **Lesion study shows that Conv in early phase of stages and MSA in late phase of stages are important for prediction**. We measure the decrease in accuracy after removing one unit from the trained model. In this experiment, we observe that the accuracy changes periodically. White, gray, and blue areas are Conv/MLP, MSA, and subsampling layers, respectively.

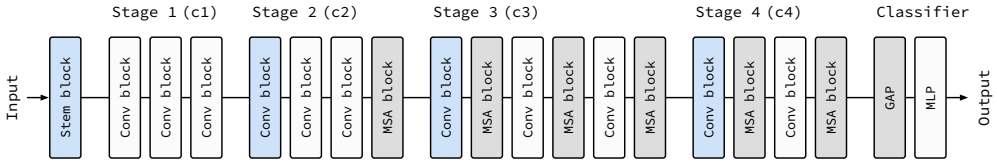

Figure D.5: **Detailed architecture of Alter-ResNet-50 for ImageNet-1K.** White, gray, and blue blocks mean Conv, MSA, and subsampling blocks. This model alternately replaces Conv blocks with MSA blocks from the end of stages. Following Swin, MSAs in stages 1 to 4 use 3, 6, 12, and 24 heads, respectively. We use 6 MSA blocks for ImageNet since large amount of data alleviates the drawback of MSA. See Fig. 11 to compare with the model for CIFAR-100.

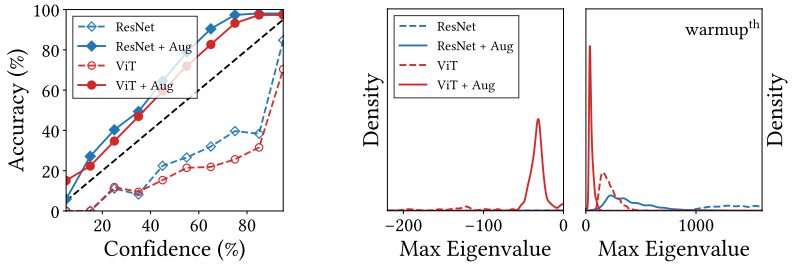

(a) Reliability diagram (b) Hessian max eigenvalue spectra

Figure F.1: **Distinctive properties of strong data augmentation.** "Aug" stands for strong data augmentation. *Left:* Strong data augmentation makes predictions underconfident on CIFAR-100. We observe the same phenomenon on ImageNet-1K. *Right:* Strong data augmentation significantly reduces the magnitude of Hessian max eigenvalues. It means that the data augmentation helps NNs converge to better optima by flattening the loss landscapes. On the other hand, the data augmentation allows a lot of negative Hessian eigenvalues, i.e., it makes the loss non-convex.

E Extended Information of AlterNet

This section provides further informations on AlterNet.

Detailed architecture of AlterNet. Section 4 introduces AlterNet to harmonize Convs with MSAs. Since most MSAs take pre-activation arrangement, pre-activation ResNet is used as a baseline for consistency. We add one CNN block to the last stage of ResNet to make the number of blocks even. A local MSA from Swin is used for AlterNet. However, for simplicity of implementation, we do not implement detailed techniques, such as a cyclic shift and layer-specific initialization. For CIFAR, the patch size of the MSA is 1×1 and the window size is 4×4. If all Conv blocks are alternately replaced with MSA, AlterNet becomes a Swin-like model.

In order to achieve better performance, NNs should strongly aggregate feature maps at the end of models as discussed in Section 3 and Section 4. To this end, AlterNet use 3, 6, 12, 24 heads for MSA in each stage.

The computational costs of Conv block and MSA block are almost the same. The training throughput of Alter-ResNet-50 is 473 image/sec on CIFAR-100, which is 20% faster than that of pre-activation ResNet-50.

The optimal number of MSAs depends on the model and dataset, so we empirically determine the number of MSAs as shown in Fig. 12a. A large dataset allows a large number of MSAs. For ImageNet, we use 6 MSAs as in Fig. D.5, because large datasets alleviate the shortcoming of MSA.

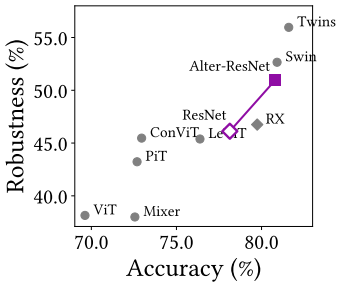

Figure E.1: **MSA with the appropriate building-up rules significantly improves ResNet** on ImageNet. Robustness is mean accuracy on ImageNet-C. "RX" is ResNeXt.

MSAs improve the performance of CNN on ImageNet. Since MSA complements Conv, MSA improves the predictive performance of CNN with the appropriate building-up rules as shown in Section 4.1. Figure E.1 reports the accuracy and robustness—mean accuracy on ImageNet-C—of CNNs and ViTs on ImageNet-1K. Since ImageNet is large dataset, a number of ViTs outperform CNNs. MSAs with the building-up rules significantly improves ResNet, and AlterNet shows competitive performance without heavy modifications. AlterNet is easy-to-implement and has a strong potential for future improvements.

F Distinctive Properties of Data Augmentation

This section empirically demonstrates that NN training with data augmentation is different from training on large datasets. We compare DeiT-style strong data augmentation with weak data augmentation, i.e., resize and crop.

F.1 Data Augmentation Can Harm Uncertainty Calibration

Figure F.1a shows the reliability diagrams of NNs with and without strong augment on CIFAR-100. In the results, both ResNet and ViT without data augmentation predict overconfident results. Data augmentation makes the predictive results under-confident (cf. Wen et al. (2021)). These are unexpected results because the predictions are not under-confident on large datasets such as ImageNet. We leave a detailed investigation for future work.

F.2 Data Augmentation Reduces the Magnitude of Hessian Eigenvalues

How does data augmentation help MSA avoid overfitting on training dataset and achieve better accuracy on test dataset? Figure F.1b shows the Hessian max eigenvalue spectra of NNs with and without strong data augmentation. First of all, data augmentation reduces the magnitude of Hessian eigenvalues, i.e., data augmentation flattens the loss landscapes in an early phase of training. The flat loss leads to better generalization. On the other hand, data augmentation allows a lot of negative Hessian eigenvalues, i.e., data augmentation makes the loss non-convex. This prevents NN from converging to a low loss on training datasets. It is clearly different from the effect of large datasets discussed in Fig. 4—large datasets convexify the loss landscapes. We leave a detailed investigation for future work.